Diffusivities and Viscosities of Poly(ethylene oxide) Oligomers†

Bingbing Hong,‡ Fernando Escobedo,§ and Athanassios Z. Panagiotopoulos*,‡

Department of Chemical Engineering, Princeton University, Princeton, New Jersey 08544, and School of Chemical and Biomolecular Engineering, Cornell University, Ithaca, New York 14853

Diffusivities and viscosities of poly(ethylene oxide) (PEO) oligomer melts with 1 to 12 repeat units have been obtained from equilibrium molecular dynamics simulations using the TraPPE-UA force field. The simulations generated diffusion coefficients with high accuracy for all of the molar masses studied, but the statistical uncertainties in the viscosity calculations were significantly larger for longer chains. There is good agreement of the calculated viscosities and densities with available experimental data, and thus, the simulations can be used to bridge gaps in the data and for extrapolations with respect to chain length, temperature, and pressure. We explored the convergence characteristics of the Green−Kubo formulas for different chain lengths and propose minimal production times required for convergence of the transport properties. The chain-length dependence of the transport properties suggests that neither Rouse nor reptation models are applicable in the short-chain regime investigated.

1. Introduction

Poly(ethylene oxide) (PEO) oligomers have applications as surfactants,[1] polymer electrolytes,[2] and drug delivery carriers in medical and biological areas.[3] They are also frequently used as model systems in connecting theories and experiments in polymer physics.[4,5] Recently, two new classes of novel hybrid materials have been developed, namely, nanoparticle ionic materials (NIMs)[6,7] and nanoparticle organic hybrid materials (NOHMs);[8] repeating "oxyethylene" structures are an important component of these materials and contribute to their unique dynamic and transport properties. Establishment of accurate structure−property relations of pure PEO forms the basis for the development of new composites in which PEO or its oligomers are a major constituent.

During the past decade, molecular simulations have frequently been used to model PEO chains. Different force fields have been studied, including those based on quantum chemistry,[9] OPLS,[10] and TraPPE and its variations.[11−13] Prior studies have reported good agreement between simulation predictions and experimental results for conformer populations,[10,11,14] spectra,[15−17] thermodynamic properties,[12,13,18] and structural relaxations.[9,19] While many atomistic simulations have investigated monodisperse PEO melts of low to moderate molar mass, there are relatively few studies of higher-molar-mass PEO as polydisperse mixtures[13] or in solution.[20] Structural properties and diffusivities of aqueous PEO mixtures are also frequently studied to test the transferability of force fields and coarse-graining techniques.[11,21−23]

In contrast to the extensive investigations of static properties, studies of PEO chain dynamics have generally been limited by the long time necessary for motion decorrelation on longer length scales. Dynamic properties explored most frequently are the local correlations of bond, segmental, and subchain motions, which relax on time scales of (10 to 100) ps.[9,11,13,16,18,19] Prior diffusivity calculations have been limited to melts of short chains or aqueous solutions of oligomers[5,9,11] because diffusivity relates to the slower dynamics of whole chains. Few studies have looked into the properties of long PEO chains in the bulk.[13] As a property determined by collective chain motions, viscosity has been even less explored using atomistic models, with values reported at only a few state points for 12-mers.[9] It is thus worthwhile to use current force fields to obtain systematic information about the transport properties of PEO, especially their dependence on chain length, despite the need for long simulation times.

Transport coefficients can be obtained through either equilibrium methods, which use fluctuation−dissipation formulas, or nonequilibrium methods that measure the response of the system to external perturbations.[24−26] Equilibrium methods are free from the theoretical and practical issues affecting nonequilibrium methods, such as temperature inhomogeneities induced by the perturbation[27] and the validity of schemes for extrapolation to the equilibrium state.[28] On the other hand, equilibrium methods have convergence problems in applications to systems characterized by slow relaxations. Previous papers have either reported the successful application of the Green−Kubo (GK) formalism to simple systems[29−34] or merely stated qualitatively the difficulty of converging the GK integrals for large molecules.[24,25,35] They have not quantitatively explored the limits of convergence for chains as a function of their length.

In this work, the TraPPE-UA force field[36,37] with a corrected dihedral potential[11,38] was chosen for simulations of $CH_3O(CH_2CH_2O)_nCH_3$ for chain lengths n from 1 to 12. Diffusion coefficients and viscosities were obtained using equilibrium methods. This study provides a test of the applicability of the TraPPE force field, which was originally parametrized with phase-equilibrium properties of small molecules, to the transport properties of chains. Unlike previous simulation studies,[9,11,13] which have reported viscosity data for a single chain length or diffusivities for low-molar-mass chains, here we systematically studied the chain-length dependence of these two transport properties. In addition, we sought to quantify the GK integration divergence for longer chains on the basis of the relative errors of the calculated transport properties.

† Part of the "Sir John S. Rowlinson Festschrift".
* Author for correspondence. E-mail: azp@princeton.edu.
‡ Princeton University.
§ Cornell University.

10.1021/je100430q
Published on Web 06/22/2010

Table 1. Simulation Parameters

		κ_T	L^d
n	N	10^{-4} MPa^{-1}	nm
1	216	11.15[60]	3.34570[a] (296.15 K, 0.1 MPa)
			3.3390[a] (298.15 K, 0.1 MPa)
			3.3534[a] (303.15 K, 1 MPa)
3	216	7.31[61]	4.0300[a] (303.15 K, 1 MPa)
5	50	6.6[61]	2.7880[a] (303.15 K, 1 MPa)
	200		4.4257[a] (303.15 K, 1 MPa)
	400		5.5760[a] (303.15 K, 1 MPa)
9	150	5.5[c]	4.7070[a] (303.15 K, 1 MPa)
			4.7114[a] (318 K, 0.1 MPa)
12	100	5.0[c]	4.4819[b] (298.15 K, 0.1 MPa)
			4.4672[b] (303.15 K, 1 MPa)

[a] Determined according to the experimental density. [b] Determined from the *NPT* simulation density. [c] Extrapolated from $n = 1$ to 5. [d] The temperature and the pressure given in parentheses are the experimental state points at which the density was reached.

The paper is organized as follows. Section 2 describes the model details and simulation methodology. Section 3 presents the calculated volumetric and transport properties as functions of chain length and compares the results with experimental data and theoretical predictions. The feasibility of transport property calculations using GK methods for longer chains is also discussed in this section. Finally, section 4 summarizes the conclusions from this work.

2. Methods

2.1. Simulation Details and Potential Models. All of the simulations were performed using GROMACS version 4.0.3.[39] Each $CH_3O(CH_2CH_2O)_nCH_3$ system with n from 1 to 12 was simulated in the *NPT* ensemble at a pressure of (0, 0.1, or 1) MPa for an initial simulation time of (3 to 18) ns, depending on the chain length. Strictly speaking, zero pressure corresponds to a metastable liquid; however, for liquids far from the critical point, the difference in the densities of the liquid at the saturation (vapor) pressure and zero pressure is negligible, and simulated systems started from liquid densities never vaporized. The density averaged over the last one-third of each simulation was compared with experimental values as a measure of accuracy for the chosen force field. Each system was then reset at the experimental density (except for 12-mers), and simulations in the *NVT* ensemble were performed for transport property calculations using equilibration times from (1 to 120) ns and production times from (2 to 40) ns, with longer simulations used for higher molar masses. Table 1 gives the input parameters for the simulations, namely, the number of chains (N), the compressibility (κ_T) used for the barostat in the NPT runs, and the simulation box size (L) for the *NVT* runs, for each chain length studied.

The configurations were updated via the leapfrog algorithm[40] using a time step of 2 fs. The system pressure was coupled to a Parrinello−Rahman barostat[41,42] with a relaxation time of 5 ps, and the compressibilities for different chain systems were set as shown in Table 1. The Nosé−Hoover thermostat[43,44] with a relaxation time of 2.5 ps was used to maintain the system at temperatures around 300 K. Interpolation between the experimental melting points for long PEO chains[45] and oligomers ($n \leq 4$)[46] and the chain lengths covered in our simulations suggested a melting point a little below or around 300 K. Hence, under the assumption that the force fields we used give melting points not far away from the corresponding experimental values, all of the simulated systems were in the stable liquid region.

Interactions between the three types of united atoms in the chains (i.e., CH_3, CH_2, and O) were described by the TraPPE-UA force field,[36,37] a set of transferable potentials developed via fitting to the liquid−vapor coexistence curves of pure substances. Nonbonded interactions in TraPPE-UA include pairwise Lennard-Jones (LJ) and Coulombic potentials. The like-pair LJ diameters (σ) and well depths (ε) were $\sigma(CH_3) = 0.375$ nm, $\sigma(CH_2) = 0.395$ nm, $\sigma(O) = 0.280$ nm and $\varepsilon(CH_3) = 0.8148$ kJ·mol^{-1}, $\varepsilon(CH_2) = 0.3825$ kJ·mol^{-1}, $\varepsilon(O) = 0.4593$ kJ·mol^{-1}. Unlike-pair interaction parameters were obtained from the Lorentz−Berthelot combining rules[26] (arithmetic mean for the diameters and geometric mean for the well depths). Partial charges of $0.25e$, $0.25e$, and $-0.50e$ were used for the CH_3, CH_2 and O centers, respectively. Both van der Waals and electrostatic interactions were truncated at 0.9 nm. The LJ interactions within the cutoff were determined between a central atom and the atoms stored in a Verlet neighbor list that was updated every 10 fs, while long-tail dispersion corrections were treated analytically.[26] The long-range electrostatics were calculated via the particle-mesh Ewald method[47,48] using fourth-order interpolation and a Fourier grid spacing of 0.12 nm. Nonbonded interactions between beads separated by three or fewer bonds within one molecule were not present, as these effects have been incorporated into the angle and torsional potential parameters. Bond lengths were fixed at 0.154 nm for CH_x-CH_y (x, $y = 2$, 3) and 0.141 nm for CH_x-O using the SHAKE algorithm with a relative tolerance of 10^{-4}. Harmonic bond bending potentials were modeled as $u_{ijk} = k_\theta(\theta_{ijk} - \theta_0)^2$, where θ_{ijk} is the angle between the three consecutive atoms along two bonds. The force constant k_θ and equilibrium angle θ_0 were $k_\theta = 502.194$ kJ·mol^{-1} and $\theta_0 = 112°$ for CH_x-O-CH_y and $k_\theta = 418.218$ kJ·mol^{-1} and $\theta_0 = 112°$ for CH_x-CH_y-O.

Fischer et al[11,38] suggested a modification of the torsional potentials in the TraPPE-UA force field in order to match the conformer population distribution to ab initio data for 1,2-dimethoxyethane (DME, $n = 1$). The new torsion potential function in the modified TraPPE potential is given by eq 1:

$$u_{\text{torsion}}(\phi) = \sum_{i=0}^{7} k_i[1 + \cos(i\phi)] \quad (1)$$

The values of the parameters k_i are listed in Table 2. For small molecules (e.g., DME), TraPPE and modified TraPPE are approximately equivalent with respect to the experimental liquid−vapor coexistence curves: over the temperature range of available experimental data,[49] the original TraPPE force field overestimates the saturated liquid density of DME by (1 to 2) %,[37] while the modified TraPPE underestimates it by around 2 %.[11,50] Differences between the two force fields increase with the number of $-CH_2CH_2O-$ units.

Figure 1 presents our results for the $\rho-P-T$ relationship in dodecaethylene glycol dimethyl ether [$(EO)_{12}$DME, $n = 12$] at (0 and 100) MPa using the two force fields. The simulation statistical uncertainties (error bars), which were obtained by dividing the samples at each state point into 10 blocks, are smaller than the symbols. Also included in Figure 1 are the experimentally measured curves[51] for poly(ethylene oxide) dimethyl ether (PEODME) mixtures with a number-average molar mass (M_n) of about 0.6 kg·mol^{-1}. The data are better reproduced by the modified TraPPE potential over the entire temperature range at both pressures. The experimental data at 0.1 MPa[9] for PEODME with $M_n \approx 0.398$ kg·mol^{-1} are represented by triangles in Figure 1; these should have negligible differences from data at 0 MPa because of the small compressibility. The system we simulated consisted of monodisperse chains having a molar mass between the M_n values of the two experimental systems. We thus confirmed that the modified

Table 2. Dihedral Parameters in the Modified TraPPE-UA Force Field

	k_i/(kJ·mol^{-1})							
	$i = 0$	1	2	3	4	5	6	7
$CH_x-O-CH_y-CH_y$	−0.25390	−5.15997	−0.69711	5.35013	0.80312	0.28307	0.09526	−0.05797
$O-CH_x-CH_x-O$	−7.75967	7.58526	6.70523	8.40071	0.63221	0.11063	0.35962	0.01683

TraPPE force field better reproduces the volumetric properties of PEO, and we employed it in the simulations of transport properties presented here.

2.2. Diffusivity and Viscosity Calculations. The diffusion coefficient can be obtained using two equivalent equilibrium methods.[26] The Green−Kubo (GK) integration over the velocity autocorrelation function is given by eq 2:

$$D = \frac{1}{3}\int_0^\infty \langle v_i(t + t_0)\cdot v_i(t_0)\rangle \, dt \tag{2}$$

In the Einstein relation, the diffusion coefficient is related to the slope of the mean-square displacement (MSD) of one particle over time:

$$D = \frac{1}{6}\lim_{t\to\infty}\frac{d}{dt}\langle[\mathbf{r}_i(t + t_0) - \mathbf{r}_i(t_0)]^2\rangle \tag{3}$$

where $\mathbf{r}_i(t)$ is the coordinate of the center of mass of the ith molecule at time t. The averages in eqs 2 and 3 are over different time origins and particles in the system. To fully capture the shape of this correlation function from our simulations, velocity files were stored every 0.1 ps when GK integration was used. The sampling frequency could be considerably reduced using eq 2, as the transition from the subdiffusive region to the diffusive region observed from the MSD is less abrupt than the fluctuation of the velocity autocorrelation function. Center-of-mass positions were sampled every 1 ps.

Similarly, equilibrium methods for shear viscosity determination include (1) GK integration over the autocorrelation function of $P_{\alpha\beta}$, the off-diagonal elements of the pressure tensor (eq 4),

$$\eta = \frac{V}{k_B T}\int_0^\infty \langle P_{\alpha\beta}(t + t_0)\cdot P_{\alpha\beta}(t_0)\rangle \, dt \tag{4}$$

and (2) the MSD of $L_{\alpha\beta}$, where $L_{\alpha\beta}$ is defined as

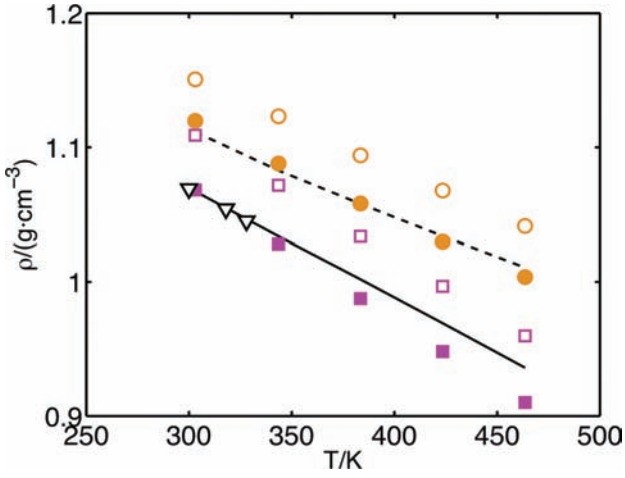

Figure 1. Density vs temperature for $(EO)_{12}DME$: ■, modified TraPPE at 0 MPa; ●, modified TraPPE at 100 MPa; □, TraPPE at 0 MPa; ○, TraPPE at 100 MPa; solid line, experimental data for PEODME ($M_n \approx 0.6$ kg·mol^{-1} and $M_w/M_n = 1.06$, where M_w is the weight-average molar mass) at 0 MPa;[51] dashed line, experimental data for PEODME ($M_n \approx 0.6$ kg·mol^{-1}, $M_w/M_n = 1.06$) at 100 MPa;[51] ▽, experimental data for PEODME ($M_n \approx 0.398$ kg·mol^{-1}, $M_w/M_n = 1.16$) at 0.1 MPa.[9]

$$L_{\alpha\beta}(t) = \sum_{i=1}^{N} r_{i\alpha}(t)p_{i\beta}(t) \tag{5}$$

where $p_{i\beta}$ is the β-component of the momentum of atom i. The average in eq 4 is taken over different time origins t_0. In applications to systems with periodic boundary conditions, the second method needs to be modified to remove discontinuities when a particle jumps across the boundary.[52,53] Recently, an adaptation of eq 5 has been derived and tested for systems where all of the potentials obey the minimum-image convention.[53] Because the relevant modifications of such a method to handle electrostatic interactions are still unclear, in this work only the boundary-condition-independent GK integral of eq 4 was used. Fully capturing the fastest vibrational mode of the pressure correlation function required $P_{\alpha\beta}$ to be sampled every 0.01 ps. To gain higher accuracy, the right-hand side of eq 4 was further averaged over the three off-diagonal elements, since PEO melts are isotropic (the isotropy was confirmed during our simulations).

The statistical errors of the quantities in eqs 2 to 4 were obtained by dividing the time origins into $N_b = 5$ blocks for the diffusion coefficient calculation and $N_b = 10$ blocks for the viscosity calculation. For each block i, we averaged the correlation functions or MSD over the time origins in i and used eqs 2 and 3 to obtain the self-diffusion coefficient or viscosity, denoted as x_i in eq 6. The statistical uncertainty with 95 % confidence (Er) was then determined using

$$Er = 2\left[\frac{\sum_{i=1}^{N_b}(x_i - \bar{x})^2}{N_b(N_b - 1)}\right]^{1/2} \tag{6}$$

where $\bar{x}$ is the mean of the series x_i.

2.3. System Size Effects. We performed *NPT* and *NVT* simulations on systems with 50 and 400 $(EO)_5DME$ chains in addition to the base case of 200 $(EO)_5DME$ chains. The system sizes and calculated transport properties for all of the systems studied are shown in Tables 1 and 3, respectively. The statistical uncertainties in the densities, viscosities, and diffusivities tended to decrease with system size. Differences between the calculated values for different sizes were within the statistical uncertainties, indicating that system size effects on the data presented in this paper are not significant.

3. Results and Discussion

3.1. Calculation of Transport Properties. As indicated by eq 4, viscosity is the value to which the integration converges at infinite time. The pressure autocorrelation functions were obtained from averaging over different time origins separated by a 10 fs interval. Figure 2 presents the normalized values of the $P_{\alpha\beta}$ ($\alpha\beta = xy, xz, yz$) correlation functions for DME and $(EO)_{12}DME$ at $T = 303.15$ K at the experimental $P = 1$ MPa densities. The curves representing the three directions have perfect overlap with each other on the scale of the graph, confirming that the system is isotropic. Figure 2a gives the autocorrelation functions at short times. A comparison between the two panels in Figure 2a shows that the fastest vibration

Table 3. Densities (ρ), Viscosities (η), and Diffusivities (D) of $CH_3O(CH_2CH_2O)_nCH_3$ (n = 1 to 12)

		ρ/(g·cm^{-3})[a]		η/(mPa·s)		D/(10^{-5} cm^2·s^{-1})	
n	state point	sim[b]	exptl[c]	sim	exptl	sim	exptl
1	296.15 K, 0.1 MPa	0.852 ± 0.001	0.8631[62]			3.15 ± 0.02	3.2[11,63]
	298.15 K, 0.1 MPa	0.8481 ± 0.0008	0.8613,[64] 0.8637,[65] 0.8626[66]	0.35 ± 0.02	0.394[67]	3.13 ± 0.04	
	303.15 K, 1 MPa	0.843 ± 0.001	0.8518[68]	0.34 ± 0.07	0.402[68]	3.47 ± 0.04	
3	303.15 K, 1 MPa	0.968 ± 0.001	0.9768[68]	1.7 ± 0.4	1.761[68]	0.61 ± 0.02	
5	303.15 K, 1 MPa, N = 50	1.016 ± 0.002	1.0204[68]	4.4 ± 3.3	4.588[68]	0.15 ± 0.03	
	N = 200	1.0155 ± 0.0006		5.0 ± 2.1		0.181 ± 0.008	
	N = 400	1.0160 ± 0.0003		4.8 ± 2.5		0.187 ± 0.009	
9	303.15 K, 1 MPa	1.056 ± 0.001		16.3 ± 9.5		0.041 ± 0.005	
	318 K, 0.1 MPa	1.0398 ± 0.0006	1.054, 1.048, 1.038[9]	11.9 ± 7.0	13.34[9]	0.062 ± 0.005	
12	298.15 K, 0.1 MPa			33.3 ± 15.0		0.017 ± 0.005	
	303.15 K, 1 MPa	1.070 ± 0.001	1.067[13,d]	41.1 ± 17.3		0.018 ± 0.002	

[a] Statistical uncertainties in the last digit are displayed. [b] Simulation results. [c] Experimental data. [d] At 303.05 K, 0.1 MPa.

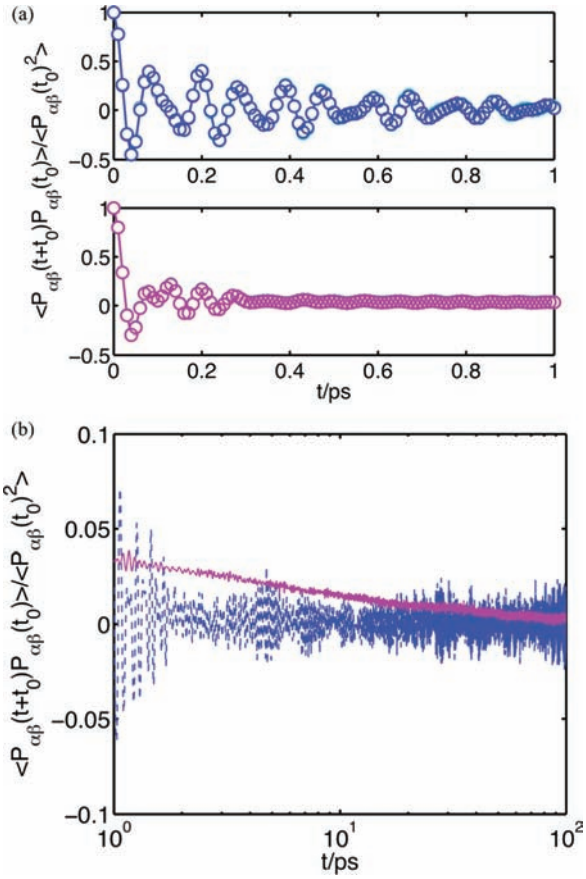

Figure 2. (a) Normalized autocorrelation functions of off-diagonal elements of the pressure tensors for (top) DME and (bottom) $(EO)_{12}$DME. The curves representing the *xy*, *xz*, and *yz* directions overlap quite well. (b) Enlarged view of the long-time tail of the pressure autocorrelation functions for DME (dashed blue line) and $(EO)_{12}$DME (solid violet line).

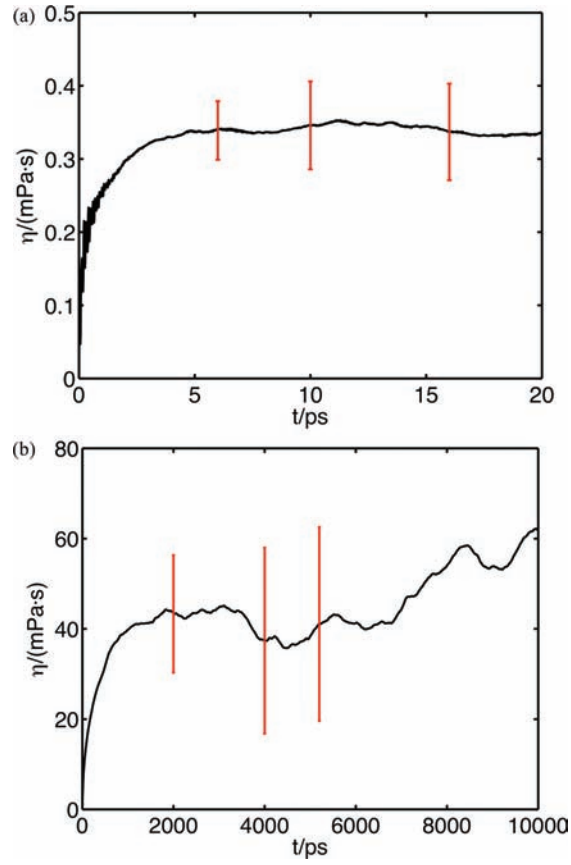

Figure 3. Effective viscosities and their statistical uncertainties vs integration time for (top) DME and (bottom) $(EO)_{12}$DME.

modes last longer than 1 ps for DME but are quickly suppressed for the longer $(EO)_{12}$DME chains. The difference arises from the fact that the backbone atoms or the shortest segments, which are responsible for the fast vibrations in $(EO)_{12}$DME, are connected to longer, more inertial backbone chains and therefore move less freely. The pressure autocorrelation functions for the two systems at long times (Figure 2b) behave in opposite ways. For the DME melt, the vibrations become small after ~3 ps and then fluctuate randomly around zero (blue line). The decay of the correlation function for the $(EO)_{12}$DME melt (violet line) decays slowly and monotonically, taking ~300 ps to reach 1 % of the value at t = 0.

The viscosity as a function of integration time is given in Figure 3 for DME and $(EO)_{12}$DME under the same conditions as for Figure 2. One would expect the viscosity to converge as the integration time increases and the pressure correlation functions decay. In practice, however, statistical noise in the long-time tail of the pressure correlation functions (Figure 2b) conceals the decay, leading to poorly converging integrals. In Figure 3, convergence is indicated by a plateau after the initial increase of the viscosity curves. The increasing error bars and deviations from the plateau at longer times for the bottom panel illustrate the poor convergence due to contributions from the noise in the long-time tails of the correlation functions. Similar behavior was also reported in a study of viscosity for the LJ liquid and SPC water.[24] Therefore, it is very important to choose a suitable integration time, which should be long enough to cover the main decay region of the pressure correlation functions

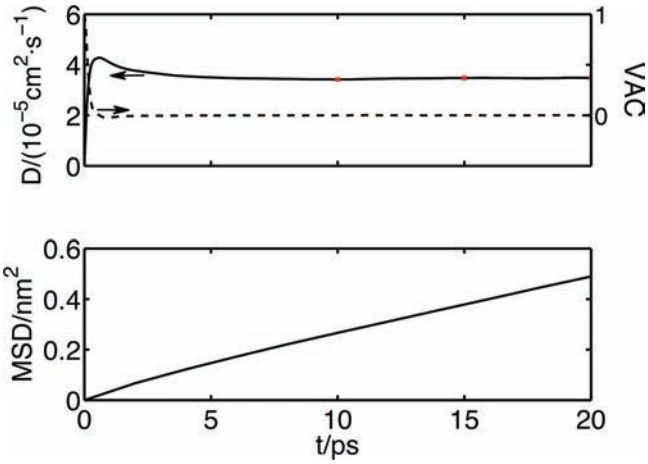

Figure 4. Calculation of the self-diffusion coefficient of DME from (top) GK integration and (bottom) the MSD method. The slope of the MSD-vs-*t* curve fitted at (10 to 20) ps is $(3.45 \pm 0.03) \cdot 10^{-5}$ cm^2·s^{-1}.

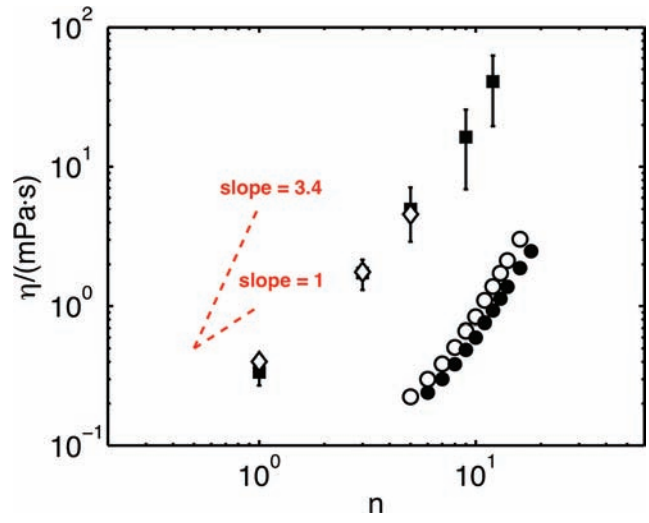

Figure 5. Chain-length dependence of the shear viscosity: ■, present simulations of $CH_3O(CH_2CH_2O)_nCH_3$ at 303.15 K, 1 MPa; ◇, experimental data for $CH_3O(CH_2CH_2O)_nCH_3$ at 303.15 K, 1 MPa;[68] ●, experimental data for *n*-alkanes at 298.15 K, 0.1 MPa;[69] ○, experimental data for *n*-alkanes at 323.15 K, 0.1 MPa.[69]

but short enough to avoid the onset of divergence. The need for a suitable integration time was also emphasized in ref 34, where viscosities of LJ fluids and water were obtained from GK calculations.

Self-diffusion coefficients were calculated using both the GK integral (eq 2) and the MSD method (eq 3). Figure 4 gives the results for DME at 303.15 K at the experimental density corresponding to a pressure of 1 MPa. Both the velocity autocorrelation function and MSD were averaged over time origins separated by 1 ps intervals, but the velocity files were stored every 0.1 ps in order to record precisely the initial decay of the correlation function. Consequently, the MSD method used 10 times less disk space than the GK integral, although the two methods are mathematically equivalent and the derivative of the MSD-versus-time curve is expected to match the integration of the velocity autocorrelation function. On the other hand, the GK method applied to diffusivity calculations has considerably better convergence (shown by the negligible error bars in the upper panel of Figure 4) than its application to viscosity calculations (integration over the pressure correlation function). This is because *D* is a one-particle property and the average of the velocity autocorrelation function in eq 2 is performed not only over time origins but also over all of the molecules involved. For DME, the GK integration could be stopped at around 7 ps, at which point the subdiffusive regime ended, but the MSD had to be recorded well beyond 7 ps before the slope of the diffusive regime was properly measured. Thus, the GK integral is preferred over the MSD method in terms of computing-time economy.

Table 3 summarizes the data obtained for density, viscosity, and diffusivity for different chain lengths. The volumetric data, as also suggested by previous studies covering a narrower range of chain lengths and conditions,[11,13,37] are in excellent agreement with available experimental data. For short chains, for which good sampling is easy to obtain, the simulated viscosities match the experimental results quite well. For longer chains, the relaxation modes in the pressure autocorrelation functions that correspond to whole-molecule motions decay slowly and become sensitive to fluctuations arising from insufficient sampling. Consequently, the errors in the simulated viscosities increase dramatically with chain length. For the longest chain, $(EO)_{12}$DME, the production period was extended to 40 ns to diminish fluctuations, but the results still had uncertainties of (40 to 50) %. Much longer simulations would have had to be used to obtain significantly more accurate predictions. For even longer chains, the simulation time necessary for good sampling becomes prohibitive given current computational resources. The table also suggests that current equilibrium-based atomistic simulations are likely only feasible for viscosity calculations in systems no more viscous than ~100 mPa·s. The relation between the uncertainties and the simulation time is discussed in section 3.3.

Experimental self-diffusion coefficients for $CH_3O(CH_2CH_2O)_nCH_3$ are not currently available for $n > 2$. On the basis of the agreement of the calculated diffusivity for DME with experimental measurements and the good match between the mean viscosity values and the experimental data, our calculated diffusivities for longer chains can be considered as predictions to be validated by future experiments. The results also indicate that modified TraPPE is a force field of good quality, giving excellent agreement with experimental data not only for the thermodynamic properties for which it was optimized but also for transport properties.

3.2. Scaling Laws. Our results for the viscosities and diffusivities of the PEO chains are plotted as functions of chain length in Figures 5 and 6, respectively. The viscosity scales with the chain length with an exponent between 1.5 and 2.4, and the diffusivity scales with an exponent between −1.9 and −2.5. In polymer theories, unentangled and entangled chain dynamics are usually described by the Rouse and reptation models, respectively, which give $\eta \propto M$, $D \propto M^{-1}$ for $M < M_c$ and $\eta \propto M^{3.3-3.4}$, $D \propto M^{-2}$ for $M > M_c$, where M_c is the critical molar mass beyond which the entanglements take effect.[54] The scaling exponent for viscosity is thus between the predicted values before and after entanglements. The relation $\eta \propto M$ (Rouse model) describes a melt of ideal chains, whereas in our simulations and experiments, the chains are driven away from ideal configurations not only by the bonded interactions (the angle and torsional potentials), which bring in stiffness, but also the nonbonded interactions, which prevent the chains from crossing each other. These interactions slow the chain motions, resulting in a more viscous system. However, the limits imposed on the chain motions by such interactions are still smaller than that of long-chain entanglements. The entanglements, as described by the reptation model, reduce the chain motions to one-dimensional movements along their contours, whereas non-

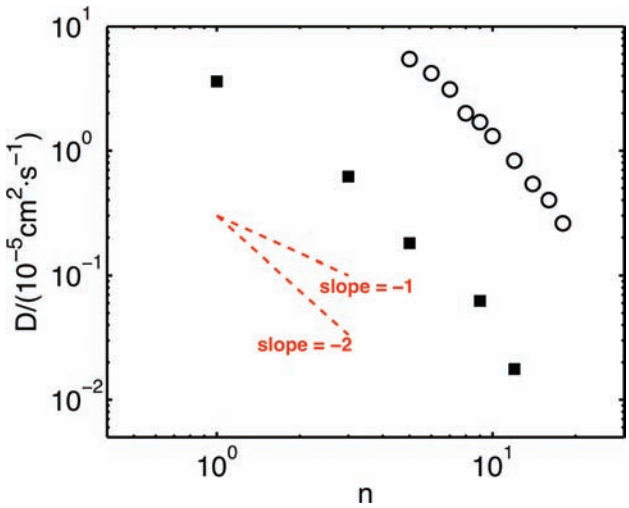

Figure 6. Chain-length dependence of the self-diffusion coefficient: ■, present simulations of $CH_3O(CH_2CH_2O)_nCH_3$ at 303.15 K, 1 MPa; ○, experimental data for *n*-alkanes at 298.15 K, 0.1 MPa.[70,71]

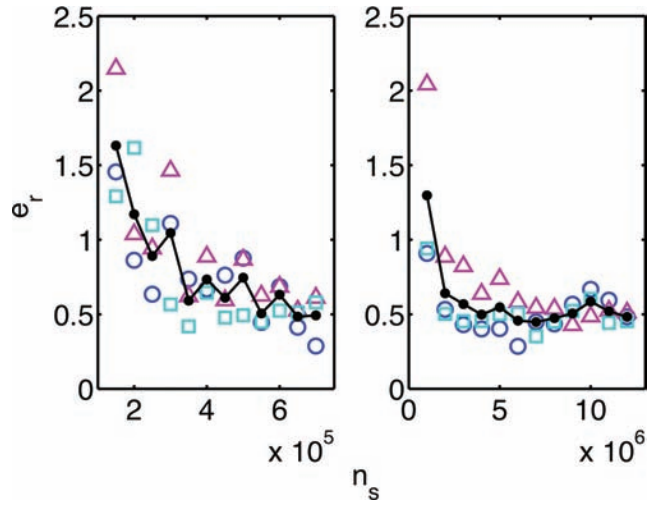

Figure 7. Relative errors (e_r) in the calculated viscosity vs number of samples (n_s) for $(EO)_5$DME (left) and $(EO)_{12}$DME (right) for an integration time of 10τ. In each panel, the symbols ○, □, and △ represent data from three independent runs under the same conditions, and the solid lines and ● symbols show the average for the three runs.

bonded interactions alone still allow chains to have freedom to move laterally. The difference explains the smaller simulated exponent in comparison with the reptation model prediction. The scaling exponent for the self-diffusion coefficient is almost the same as that of the reptation model.

We have included in Figures 5 and 6 experimental data for liquid *n*-alkanes with chain lengths *n* from 4 to 18. The viscosities and diffusivities of *n*-alkanes scale in a similar fashion to those of PEO oligomers. The closeness of the slopes suggests that inter- and intramolecular interactions play a similar role in these oligomers. Previous simulations[55,56] of fully flexible LJ-generated scaling factors [$\eta \propto n^{0.6-0.7}$ and $D \propto n^{-(0.5-0.8)}$] were significantly different from the present results, suggesting an important but still unclear effect of the chain stiffness on the scaling behavior of short chains. Although the reported exponents for the flexible chains were obtained at constant density, while in the present work we used fixed pressure, it seems unlikely that this is the cause of the discrepancy. For *n*-alkanes, it is known[57,58] that the crossover to ideal-chain statistics takes place when number of methylene groups is greater than 100. With stronger electrostatic interactions, PEO chains are expected to be stiffer. As a result, PEO needs more backbone repeat units than *n*-alkanes to have an independently rotating segment and enter the Gaussian-chain regime. The critical length of a polymer for the entanglement to take effect, however, depends in a nontrivial way on the backbone stiffness. Chain stiffness has been shown to accelerate the onset of the reptation regime for LJ chains.[59] It would be interesting to test whether that counterintuitive relation between stiffness and entanglement length remains true for longer PEO and *n*-alkane chains.

3.3. Convergence of Transport Properties. In section 3.1, we stated that the integration time in eq 4 needs to be suitably chosen in order to cover the main relaxation region of the pressure correlation functions and avoid the divergence region (large errors or deviation from the plateau). It has also been pointed out that insufficient sampling brings large fluctuations into the long-tail decay part and leads to early divergence of the integration. How can we determine whether the sampling is sufficient and whether the integration time is neither too long nor too short? There should be a relation between integration time, number of samples, and the quantity measuring the degree of divergence.

We introduce for the pressure correlation function a relaxation time τ, defined as $t_{0.1\%} - t_0$, where $t_{0.1\%}$ is the time at which the long-tail normalized correlation function is reduced to 0.1 % of the value at t_0. The relaxation times for chains with $n = 1$, 3, 5, 9, and 12 were obtained from our simulations as (3, 15, 50, 200, and 500) ps, respectively. The degree of divergence of the integration is measured by the relative error (e_r), which is defined as the ratio of the statistical uncertainty (*Er* from eq 6) for a quantity *x* to its mean value: $e_r = Er/\bar{x}$. Figure 7 presents the relation between the relative error in viscosity and the number of samples (n_s) obtained using an integration time of 10τ. Results for both the pentamer and dodecamer indicate a rapid decrease in e_r with increasing n_s when n_s is still small. Once e_r gets to around 50 %, the convergence of the GK integration cannot be improved by additional sampling as effectively as before. This flattening tendency reveals the computational difficulty of realizing better convergence (e.g., < 30 % relative error), especially for long chains.

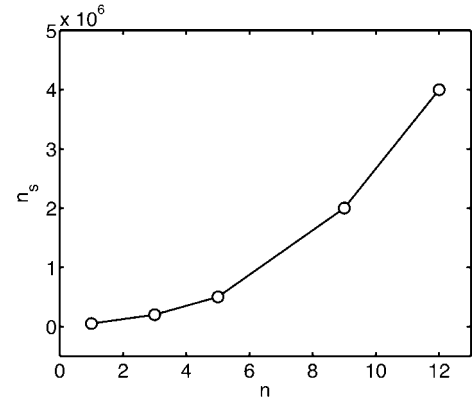

Figure 8. Number of samples (n_s) as a function of chain length *n*. This reflects an approximate relation between the minimal production time t_m and *n*.

For the choice of 60 % relative error as the point separating convergence and divergence (any choice in the 50−80 % range would give similar conclusions), the rough number of samples necessary for the GK integral to be convergent as a function of chain length is shown in Figure 8. The number of samples can be considered to be roughly proportional to CPU time, and therefore, it is an indirect measure of the minimal production time t_m needed to converge the GK integral. Fitting the data in

Figure 8 gave $t_m \propto n^{\alpha}$ with $\alpha \approx 1.2$ at the short-chain end and $\alpha \approx 2.4$ when n approaches 12. The exponents are very close to those for the $\tau \propto n^{\beta}$ relation, where τ is the relaxation time of the pressure autocorrelation function defined above and $\beta \approx 1.7$ to 2.6 as n goes from 1 to 12. The time τ can also be viewed as being roughly proportional to the time to fully equilibrate the chain melts. Assuming a characteristic monomer relaxation time of $\sim 10^{-10}$ s[16] gave a relaxation time of $\sim$80 ns for $(EO)_{12}$DME, confirming that our simulations were long enough.

In ref 26, a relation was derived for the standard error of the normalized correlation function in the form of $t_{run}^{1/2}$, where t_{run} is the length of production time. This scaling provides an alternative for estimating the minimal run length needed in order to reduce the noise in the correlation functions. It is applicable to different correlation functions and easy to use for quick estimations with any new system. However, the errors in the transport properties originate from two factors: correlation function calculation and integration. The method of ref 26 leaves the second factor unaddressed. On the contrary, though the scaling relations obtained in this paper are confined to the PEO melt system, they take into account both factors and relate the final degree of divergence directly to run length.

4. Conclusions

Atomistic molecular dynamics simulations using the modified TraPPE-UA force field have been carried out to investigate the transport properties of PEO oligomers $CH_3O(CH_2CH_2O)_nCH_3$ with $1 \leq n \leq 12$. We have demonstrated that transport properties for this class of molecules can be obtained from equilibrium molecular dynamics simulations. As a single-particle property, diffusivity could be calculated with fast convergence and high accuracy for all chain lengths of interest using the Green−Kubo formula. Viscosities, however, were less satisfactorily determined via the GK integral because of significant sampling difficulties. Although the method could be used for short chains, insufficient sampling for the pressure autocorrelation functions resulted in poor GK integral convergence. The method is not suitable for viscosity calculations of chains longer than the ones studied here.

Through the exploration of how sampling affects the convergence or relative errors, we have obtained a rough relation estimating the minimal production time necessary to obtain relative errors less than a given tolerance as a function of chain length. We have also obtained a relation between equilibrium (preproduction) time and chain length that enabled us to ensure that the systems had been fully equilibrated before the properties of interest were sampled, an issue that most prior studies have not addressed.[9,11,13,31,58] The methodology proposed here for estimating the simulation time for long chains on the basis of the scaling relation for short chains can be extended to other polymer systems. It gives useful information for assessing when the equilibrium methods are effective, when they break down, and how much additional computational effort may be required to improve the predictions.

No prior systematic investigations of viscosity or diffusivity in the melt had been performed for PEO chains. This work has obtained the chain-length dependence of viscosity and diffusivity for PEO oligomers and compared it to experimental results for PEO and to the behavior of *n*-alkanes. The similar scaling factors of the two systems reflect the influences of intra- and intermolecular interactions on the dynamics of these oligomers. In comparison with the Rouse and reptation models, the exponents also suggest that the chain lengths of interest in this paper are far from ideal-chain statistics and the region where entanglements take effect. Finally, our simulations have confirmed the applicability of the TraPPE-based force field, which has been widely tested for structural and thermodynamic properties, to transport properties of PEO melts.

Acknowledgment

This paper is dedicated to Sir John Rowlinson for his many contributions to experiment, theory, and the history of thermodynamics and for his mentorship of one of us (A.Z.P.) at a critical and formative time.

Literature Cited

(1) Drohmann, C.; Beckman, E. J. Phase behavior of polymers containing ether groups in carbon dioxide. *J. Supercrit. Fluids* **2002**, *22*, 103–110.
(2) Croce, F.; Appetecchi, G. B.; Persi, L.; Scrosati, B. Nanocomposite polymer electrolytes for lithium batteries. *Nature* **1998**, *394*, 456–458.
(3) Harris, J. M. *Poly(ethylene glycol) Chemistry: Biotechnological and Biomedical Applications*; Plenum Press: New York, 1992.
(4) Teramoto, A.; Fujita, H. Temperature and Molecular Weight Dependence of Melt Viscosity of Polyethylene Oxide in Bulk. *Makromol. Chem.* **1965**, *85*, 261–272.
(5) Shimada, K.; Kato, H.; Saito, T.; Matsuyama, S.; Kinugasa, S. Precise measurement of the self-diffusion coefficient for poly(ethylene glycol) in aqueous solution using uniform oligomers. *J. Chem. Phys.* **2005**, *122*, 244914.
(6) Bourlinos, A. B.; Giannelis, E. P.; Zhang, Q.; Archer, L. A.; Floudas, G.; Fytas, G. Surface-functionalized nanoparticles with liquid-like behavior: The role of the constituent components. *Eur. Phys. J. E* **2006**, *20*, 109–117.
(7) Rodriguez, R.; Herrera, R.; Archer, L. A.; Giannelis, E. P. Nanoscale Ionic Materials. *Adv. Mater.* **2008**, *20*, 4353–4358.
(8) Qi, H.; Agarwal, P., Archer, L. A., Time-strain superposition in suspensions of hairy nanoparticles. Submitted.
(9) Borodin, O.; Douglas, R.; Smith, G. A.; Trouw, F.; Petrucci, S. MD Simulations and experimental study of structure, dynamics, and thermodynamics of poly(ethylene oxide) and its oligomers. *J. Phys. Chem. B* **2003**, *107*, 6813–6823.
(10) Anderson, P. M.; Wilson, M. R. Developing a force field for simulation of poly(ethylene oxide) based upon ab initio calculations of 1,2-dimethoxyethane. *Mol. Phys.* **2005**, *103*, 89–97.
(11) Fischer, J.; Paschek, D.; Geiger, A.; Sadowski, G. Modeling of aqueous poly(oxyethylene) solutions: 1. Atomistic Simulations. *J. Phys. Chem. B* **2008**, *112*, 2388–2398.
(12) Tritopoulou, E. A.; Economou, I. G. Molecular simulation of structure and thermodynamic properties of pure tri- and tetra-ethylene glycols and their aqueous mixtures. *Fluid Phase Equilib.* **2006**, *248*, 134–146.
(13) Wick, C. D.; Theodorou, D. N. Connectivity-altering Monte Carlo simulations of the end group effects on volumetric properties for poly(ethylene oxide). *Macromolecules* **2004**, *37*, 7026–7033.
(14) Neyertz, S.; Brown, D.; Thomas, J. O. Molecular-Dynamics Simulation of Crystalline Poly(Ethylene Oxide). *J. Chem. Phys.* **1994**, *101*, 10064–10073.
(15) Smith, G. D.; Yoon, D. Y.; Jaffe, R. L.; Colby, R. H.; Krishnamoorti, R.; Fetters, L. J. Conformations and structures of poly(oxyethylene) melts from molecular dynamics simulations and small-angle neutron scattering experiments. *Macromolecules* **1996**, *29*, 3462–3469.
(16) Lin, B.; Boinske, P. T.; Halley, J. W. A molecular dynamics model of the amorphous regions of polyethylene oxide. *J. Chem. Phys.* **1996**, *105*, 1668–1681.
(17) Sasanuma, Y.; Ohta, H.; Touma, I.; Matoba, H.; Hayashi, Y.; Kaito, A. Conformational characteristics of poly(ethylene sulfide) and poly(ethylene oxide): Solvent dependence of attractive and repulsive gauche effects. *Macromolecules* **2002**, *35*, 3748–3761.
(18) Neyertz, S.; Brown, D.; Colombini, D.; Alberola, N. D.; Merle, G. Volume dependence of molecular flexibility in poly(ethylene oxide) under negative pressure. *Macromolecules* **2000**, *33*, 1361–1369.
(19) Neyertz, S.; Brown, D. A Computer-Simulation Study of the Chain Configurations in Poly(Ethylene Oxide)-Homolog Melts. *J. Chem. Phys.* **1995**, *102*, 9725–9735.
(20) Brodeck, M.; Alvarez, F.; Arbe, A.; Juranyi, F.; Unruh, T.; Holderer, O.; Colmenero, J.; Richter, D. Study of the dynamics of poly(ethylene oxide) by combining molecular dynamic simulations and neutron scattering experiments. *J. Chem. Phys.* **2009**, *130*, 094908.
(21) Shang, B. Z.; Wang, Z. W.; Larson, R. G. Molecular dynamics simulation of interactions between a sodium dodecyl sulfate micelle and a poly(ethylene oxide) polymer. *J. Phys. Chem. B* **2008**, *112*, 2888–2900.

(22) Smith, G. D.; Bedrov, D. A molecular dynamics simulation study of the influence of hydrogen-bonding and polar interactions on hydration and conformations of a poly(ethylene oxide) oligomer in dilute aqueous solution. *Macromolecules* **2002**, *35*, 5712–5719.
(23) Smith, G. D.; Borodin, O.; Bedrov, D. A revised quantum chemistry-based potential for poly(ethylene oxide) and its oligomers in aqueous solution. *J. Comput. Chem.* **2002**, *23*, 1480–1488.
(24) Hess, B. Determining the shear viscosity of model liquids from molecular dynamics simulations. *J. Chem. Phys.* **2002**, *116*, 209–217.
(25) Bordat, P.; Muller-Plathe, F. The shear viscosity of molecular fluids: A calculation by reverse nonequilibrium molecular dynamics. *J. Chem. Phys.* **2002**, *116*, 3362–3369.
(26) Allen, M. P.; Tildesley, D. J. *Computer Simulation of Liquids*; Oxford University Press: New York, 1987.
(27) Liem, S. Y.; Brown, D.; Clark, J. H. R. Investigation of the homogeneous-shear nonequilibrium-molecular-dynamics methods. *Phys. Rev. A* **1992**, *45*, 3706–3713.
(28) Travis, K. P.; Searles, D. J.; Evans, D. J. Strain rate dependent properties of a simple fluid. *Mol. Phys.* **1998**, *95*, 195–202.
(29) Meier, K.; Laesecke, A.; Kabelac, S. Transport coefficients of the Lennard-Jones model fluid. I. Viscosity. *J. Chem. Phys.* **2004**, *121*, 3671–3687.
(30) Meier, K.; Laesecke, A.; Kabelac, S. Transport coefficients of the Lennard-Jones model fluid. II. Self-diffusion. *J. Chem. Phys.* **2004**, *121*, 9526–9535.
(31) Yoo, C. D.; Kim, S.-C.; Lee, S. H. Viscosity and Diffusion of Small Normal and Isomeric Alkanes: An Equilibrium Molecular Dynamics Simulation Study. *Bull. Korean Chem. Soc.* **2008**, *29*, 1059–1062.
(32) Rey-Castro, C.; Vega, L. F. Transport properties of the ionic liquid 1-ethyl-3-methylimidazolium chloride from equilibrium molecular dynamics simulation. The effect of temperature. *J. Phys. Chem. B* **2006**, *110*, 14426–14435.
(33) Rey-Castro, C.; Vega, L. F. Transport properties of the ionic liquid 1-ethyl-3-methylimidazolium chloride from equilibrium molecular dynamics simulation. The effect of temperature. *J. Phys. Chem. B* **2006**, *110*, 16157–16157.
(34) Chen, T.; Smit, B.; Bell, A. T. Are pressure fluctuation-based equilibrium methods really worse than nonequilibrium methods for calculating viscosities? *J. Chem. Phys.* **2009**, *131*, 246101.
(35) Borodin, O.; Smith, G. D.; Kim, H. Viscosity of a Room Temperature Ionic Liquid: Predictions from Nonequilibrium and Equilibrium Molecular Dynamics Simulations. *J. Phys. Chem. B* **2009**, *113*, 4771–4774.
(36) Martin, M. G.; Siepmann, J. I. Transferable potentials for phase equilibria. 1. United-atom description of *n*-alkanes. *J. Phys. Chem. B* **1998**, *102*, 2569–2577.
(37) Stubbs, J. M.; Potoff, J. J.; Siepmann, J. I. Transferable potentials for phase equilibria. 6. United-atom description for ethers, glycols, ketones, and aldehydes. *J. Phys. Chem. B* **2004**, *108*, 17596–17605.
(38) Fischer, J.; Paschek, D.; Geiger, A.; Sadowski, G. Modeling of aqueous poly(oxyethylene) solutions: 1. Atomistic simulations. *J. Phys. Chem. B* **2008**, *112*, 8849–8850.
(39) van der Spoel, D.; Lindahl, E.; Hess, B.; van Buuren, A. R.; Apol, E.; Meulenhoff, P. J.; Tieleman, D. P.; Sijbers, A. L. T. M.; Feenstra, K. A.; van Drunen, R.; Berendsen, H. J. C. *Gromacs User Manual*, version 4.0; 2005. http://www.gromacs.org.
(40) Hockney, R. W.; Goel, S. P.; Eastwood, J. W. Quiet High-Resolution Computer Models of a Plasma. *J. Comput. Phys.* **1974**, *14*, 148–158.
(41) Parrinello, M.; Rahman, A. Polymorphic Transitions in Single-Crystals—A New Molecular-Dynamics Method. *J. Appl. Phys.* **1981**, *52*, 7182–7190.
(42) Nose, S.; Klein, M. L. Constant Pressure Molecular-Dynamics for Molecular-Systems. *Mol. Phys.* **1983**, *50*, 1055–1076.
(43) Nose, S. A Molecular-Dynamics Method for Simulations in the Canonical Ensemble. *Mol. Phys.* **1984**, *52*, 255–268.
(44) Hoover, W. G. Canonical Dynamics—Equilibrium Phase-Space Distributions. *Phys. Rev. A* **1985**, *31*, 1695–1697.
(45) Hay, J. N. Equilibrium Melting-Point of Poly(Ethylene Oxide). *Makromol. Chem.* **1976**, *177*, 2559–2561.
(46) Linstrom, P. J.; Mallard, W. G., Eds. *NIST Chemistry WebBook*; NIST Standard Reference Database No. 69; National Institute of Standards and Technology: Gaithersburg, MD; webbook.nist.gov/chemistry (accessed March 27, 2010).
(47) Darden, T.; York, D.; Pedersen, L. Particle Mesh Ewald: An $N \cdot \log(N)$ Method for Ewald Sums in Large Systems. *J. Chem. Phys.* **1993**, *98*, 10089–10092.
(48) Essmann, U.; Perera, L.; Berkowitz, M. L.; Darden, T.; Lee, H.; Pedersen, L. G. A Smooth Particle Mesh Ewald Method. *J. Chem. Phys.* **1995**, *103*, 8577–8593.
(49) Properties of Organic Compounds. http://www.chemnetbase.com/scripts/pocweb.exe (accessed March 27, 2010).
(50) Ku, H. C.; Tu, C. H. Densities and viscosities of seven glycol ethers from 288.15 to 343.15 K. *J. Chem. Eng. Data* **2000**, *45*, 391–394.
(51) Zoller, P.; Walsh, D. J., *Standard Pressure−Volume−Temperature Data for Polymers*; Technomic Publishing Co.: Lancaster, PA, 1995.
(52) Erpenbeck, J. J. Einstein−Kubo−Helfand and Mcquarrie Relations for Transport-Coefficients. *Phys. Rev. E* **1995**, *51*, 4296–4308.
(53) Viscardy, S.; Servantie, J.; Gaspard, P. Transport and Helfand moments in the Lennard-Jones fluid. I. Shear viscosity. *J. Chem. Phys.* **2007**, *126*, 184512.
(54) de Gennes, P. G. *Scaling Concepts in Polymer Physics*; Cornell University Press: Ithaca, NY, 1979.
(55) Galliero, G.; Boned, C. Shear viscosity of the Lennard-Jones chain fluid in its gaseous, supercritical, and liquid states. *Phys. Rev. E* **2009**, *79*, 021201.
(56) Reis, R. A.; Silva, F. C.; Nobrega, R.; Oliveira, J. V.; Tavares, F. W. Molecular dynamics simulation data of self-diffusion coefficient for Lennard-Jones chain fluids. *Fluid Phase Equilib.* **2004**, *221*, 25–33.
(57) Brown, D.; Clarke, J. H. R.; Okuda, M.; Yamazaki, T. A Molecular-Dynamics Study of Chain Configurations in *n*-Alkane-Like Liquids. *J. Chem. Phys.* **1994**, *100*, 1684–1692.
(58) Lee, S. H.; Chang, T. Y. Viscosity and diffusion constants calculation of *n*-alkanes by molecular dynamics simulations. *Bull. Korean Chem. Soc.* **2003**, *24*, 1590–1598.
(59) Faller, R.; Muller-Plathe, F. Chain stiffness intensifies the reptation characteristics of polymer dynamics in the melt. *ChemPhysChem* **2001**, *2*, 180–184.
(60) Benson, G. C.; Wang, L. L.; Lu, B. C. Y. Excess enthalpies of (heptane plus methyl 1,1-dimethylethyl ether plus 1,2-dimethoxyethane) at the temperature 298.15 K and ambient pressure. *J. Chem. Thermodyn.* **1998**, *30*, 1533–1541.
(61) Comunas, M. J. P.; Lopez, E. R.; Pires, P.; Garcia, J.; Fernandez, J. $P-\rho-T$ measurements of polyethylene glycol dimethylethers between 278.15 and 328.15 K at pressures to 12 MPa. *Int. J. Thermophys.* **2000**, *21*, 831–851.
(62) Zheng, P. J.; Meng, X. Y.; Wu, J. T.; Liu, Z. G. Density and viscosity measurements of dimethoxymethane and 1,2-dimethoxyethane from 243 to 373 K up to 20 MPa. *Int. J. Thermophys.* **2008**, *29*, 1244–1256.
(63) Bedrov, D.; Borodin, O.; Smith, G. D.; Trouw, F.; Mayne, C. Simulation and QENS studies of molecular dynamics in aqueous solutions of 1,2-dimethoxyethane. *J. Phys. Chem. B* **2000**, *104*, 5151–5154.
(64) Das, B.; Roy, M. N.; Hazra, D. K. Densities and Viscosities of the Binary Aqueous Mixtures of Tetrahydrofuran and 1,2-Dimethoxyethane at 198, 308 and 318 K. *Indian J. Chem. Technol.* **1994**, *1*, 93–97.
(65) Kusano, K. Densities, Refractive Indexes, and Normal Boiling Points of 1,2-Disubstituted Ethylene Glycol Derivatives. *J. Chem. Eng. Data* **1978**, *23*, 141–143.
(66) Pal, A.; Sharma, S. Excess molar volumes and viscosities of 1-propanol + ethylene glycol, + ethylene glycol monomethyl, + ethylene glycol dimethyl, + diethylene glycol dimethyl, + triethylene glycol dimethyl, + diethylene glycol diethyl, and + diethylene glycol dibutyl ethers at 298.15K. *J. Chem. Eng. Data* **1998**, *43*, 532–536.
(67) Ku, H. C.; Tu, C. H. Densities and viscosities of binary and ternary mixtures of ethanol, 2-butanone, and 2,2,4-trimethylpentane at $T =$ (298.15, 308.15, and 318.15) K. *J. Chem. Eng. Data* **2005**, *50*, 608–615.
(68) Conesa, A.; Shen, S.; Coronas, A. Liquid densities, kinematic viscosities, and heat capacities of some ethylene glycol dimethyl ethers at temperatures from 283.15 to 423.15 K. *Int. J. Thermophys.* **1998**, *19*, 1343–1358.
(69) Lide, D. R., Ed. *CRC Handbook of Chemistry and Physics*, 90th ed. (Internet version 2010); CRC Press/Taylor and Francis: Boca Raton, FL, 2010; www.hbcpnetbase.com (accessed March 27, 2010).
(70) Douglass, D. C.; McCall, D. W. Diffusion in Paraffin Hydrocarbons. *J. Phys. Chem.* **1958**, *62*, 1102–1107.
(71) Ertl, H.; Dullien, F. A. L. Self-Diffusion and Viscosity of Some Liquids as a Function of Temperature. *AIChE J.* **1973**, *19*, 1215–1223.

Received for review April 27, 2010. Accepted June 5, 2010. This publication is based on work supported by Award KUS-CI-018-02 made by King Abdullah University of Science and Technology (KAUST).

JE100430Q